REPORT DOCUMENTATION PAGE

Form Approved
OMB No. 0704-0188

1. REPORT DATE (DD-MM-YYYY)	2. REPORT TYPE	3. DATES COVERED (From - To)
15 May 2002	Final	Jan 01, 1999 – Dec 31, 2001

4. TITLE AND SUBTITLE
III- Nitride UV Detector Arrays Fabricated by Combining HVPE

Lateral Epitaxial Overgrowth and MBE Methods

5a. CONTRACT NUMBER

5b. GRANT NUMBER
N00014-99-1-0309

5c. PROGRAM ELEMENT NUMBER

6. AUTHOR(S)

Moustakas, Theodore D.

5d. PROJECT NUMBER
01PR01402-01

5e. TASK NUMBER

5f. WORK UNIT NUMBER

7. PERFORMING ORGANIZATION NAME(S) AND ADDRESS(ES)

Boston University
Electrical and Computer Eng.
8 Saint Mary's St.,
Boston. MA 02215

8. PERFORMING ORGANIZATION REPORT NUMBER

9. SPONSORING / MONITORING AGENCY NAME(S) AND ADDRESS(ES)
Office Of Naval Research 312
Ballston Center Tower One
800 North Quincy St.,
Arlington, VA 22217-5660

10. SPONSOR/MONITOR'S ACRONYM(S)

11. SPONSOR/MONITOR'S REPORT NUMBER(S)

12. DISTRIBUTION / AVAILABILITY STATEMENT

Approved for Public Release; Distribution Unlimited

20020708 080

13. SUPPLEMENTARY NOTES

14. ABSTRACT. The work focused on the fabrication of GaN and AlGaN detectors. Material studies of AlGaN alloys have been undertaken to improve the absorption characteristics and to develop films free of cracks. The devices were fabricated in the form of Schottky barriers, p-n and p-i-n junctions. To reduce the dark current in these devices, a number of approaches were investigated (use of thick GaN templates grown by the HVPE and the LEO methods, or utilized a number AlN interlayers prior to the growth of the device structure). A lithographic mask set was developed for the deposition of detector arrays with various configurations. High quantum efficiency (70%) Schottky barriers with five orders of magnitude visible light rejection were fabricated. P-n and p-i-n detectors with dark current at low reverse bias of about 10^{-11} Amps/cm^2 were fabricated. Rapid thermal annealing in forming gas was found to reduce the junction leakage current by orders of magnitude. These devices were found to have gains higher than one, a result attributed to photoconductive gain in the dislocation regions.

15. SUBJECT TERMS Gallium Nitride, Aluminum Gallium Nitride, Visible blind detectors, Solar blind detectors, Schottky barriers, p-i-n diodes, Molecular Beam Epitaxy, Halide Vapor Phase Epitaxy, Lateral Epitaxial Overgrowth

16. SECURITY CLASSIFICATION OF:			17. LIMITATION OF ABSTRACT	18. NUMBER OF PAGES	19a. NAME OF RESPONSIBLE PERSON
a. REPORT	b. ABSTRACT	c. THIS PAGE			19b. TELEPHONE NUMBER (include area code)
Unclassified	Unclassified	Unclassified	Unclassified	34	

Final Technical Report

III-Nitride UV Detector Arrays Fabricated by Combining HVPE Lateral Epitaxial Overgrowth and MBE Methods

ONR Grant No. N00014-99-1-0309

(January 01, 1999 – December 31, 2001)

P.I. Theodore D. Moustakas

Department of Electrical and Computer Engineering
Boston University
Boston, MA 02215
617-353-5431

May 15, 2002

Table of Contents

1. Program Goals and Objectives

The goals of this program are to develop solar-blind and visible-blind UV detectors and arrays based on III-V Nitrides with low noise equivalent power (NEP). Towards this goal, a number of material studies of AlGaN alloys have been undertaken in order to develop material with sharp absorption characteristics and improve the visible light rejection of these devices. Furthermore, GaN thick films produced by the halide vapor phase epitaxy (HVPE) method are used as substrates for these studies in order to reduce the dislocation density in the active region of the device and thus improve its noise characteristics. Heterojunction device designs are implemented to lead to high responsivity in the solar-blind region of the spectrum.

2. Experimental Results and Discussion

2.1. Development of Large Area and Low Dislocation Density GaN Substrate by the HVPE Method

Two approaches have been used in developing GaN quasi-substrates by the HVPE method. In the first method, we grew 5-10 μm thick GaN films on a (0001) sapphire substrate and in the second method we used the lateral epitaxial overgrowth (LEO)-HVPE method to further reduce the dislocation densities.

A. Development of Thick GaN Films by HVPE

Developed a new two-temperature step process (low temperature GaN buffer and high temperature GaN film) for the growth of n-GaN films by the HVPE method [1]. This was previously done only by the MOCVD and MBE methods. These films have been used as templates for the growth of the active layers of the detectors by the MBE method as described below.

The HVPE method was developed to lead to atomically smooth films on sapphire substrates. Atomic force microscopy on films ~ 4 microns thick show an rms roughness of .8 nm (~2 monolayer). An atomic force microscopy of a representative sample is shown in Figure 1.

The data in Figure 1 indicate that film has been grown in the step-flow growth mode. The step height is approximately 2 monolayers and the terraces are ~200 nm wide. Thus such atomically smooth templates are ideal for the homoepitaxial growth of active layers by MBE for the fabrication of solar blind detectors.

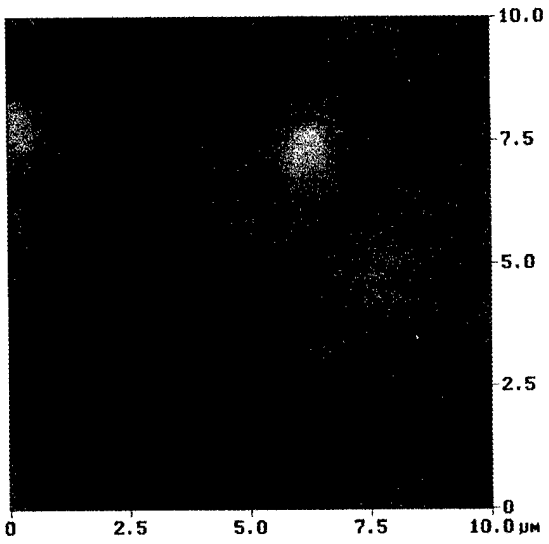

Figure 1. Atomic force microscopy of a 4 μm GaN film deposited on a (0001) sapphire substrate by the HVPE method.

The HVPE films described in Figure 1 were also characterized by photoluminescence (PL) measurements. A PL spectrum measured at room temperature is shown in Figure 2. The recombination occurs primarily across the gap at 3.41 eV and the full width at half maximum (FWHM) is 33 meV, which is close to the expected theoretical value. Thus the PL measurements also confirm that the GaN templates have excellent optical properties.

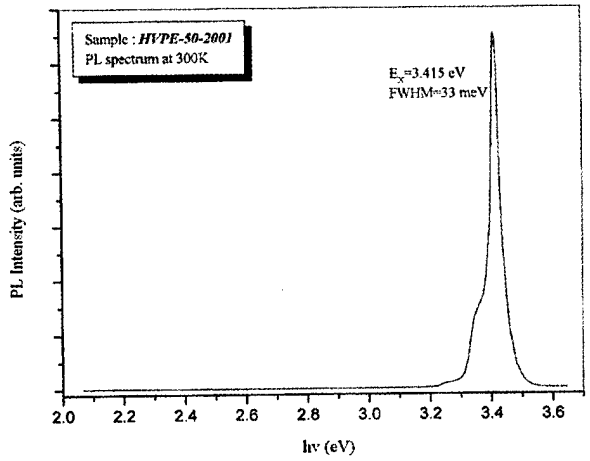

Figure 2. Photoluminescence of a 4 μm thick GaN film grown by the HVPE method using the two-temperature step process as described in the text.

The objective of homoepitaxy is to improve the quality of the MBE deposited epilayer by employing a template that has a lower dislocation density than films deposited using the three-step growth technique. This process can be advantageous even when using relatively thin templates (2-5 μm) because films grown by the HVPE or MOCVD methods generally have an order of magnitude fewer dislocations than similar films deposited by MBE. The HVPE films were grown at Boston University using a horizontal quartz reactor by flowing HCl over Ga melt that produces GaCl. Using N_2 as a carrier gas, the GaCl is transported to the substrate where it reacts with NH_3 and forms GaN. The films used were typically unintentionally doped n-type with carrier concentration between $5x10^{18}$ to $1x10^{19}$ cm^{-3}. The density of dislocations in our thin GaN templates was estimated from photo-assisted electrochemical etching, hot 3:1 H_2SO_4: H_3PO_4 etching as well as transmission electron microscopy (TEM) to be on the order of ~ 10^8 cm^{-2}. Figure 3 shows a cross-sectional TEM micrograph of a representative HVPE GaN template. These films have been determined to be Ga-polar based on KOH etching experiments. The TEM data of Figure 3 shows a very defective region next to the sapphire substrate for approximately half a micron. This defective region corresponds to the low temperature buffer, which was employed for the growth of this HVPE material.

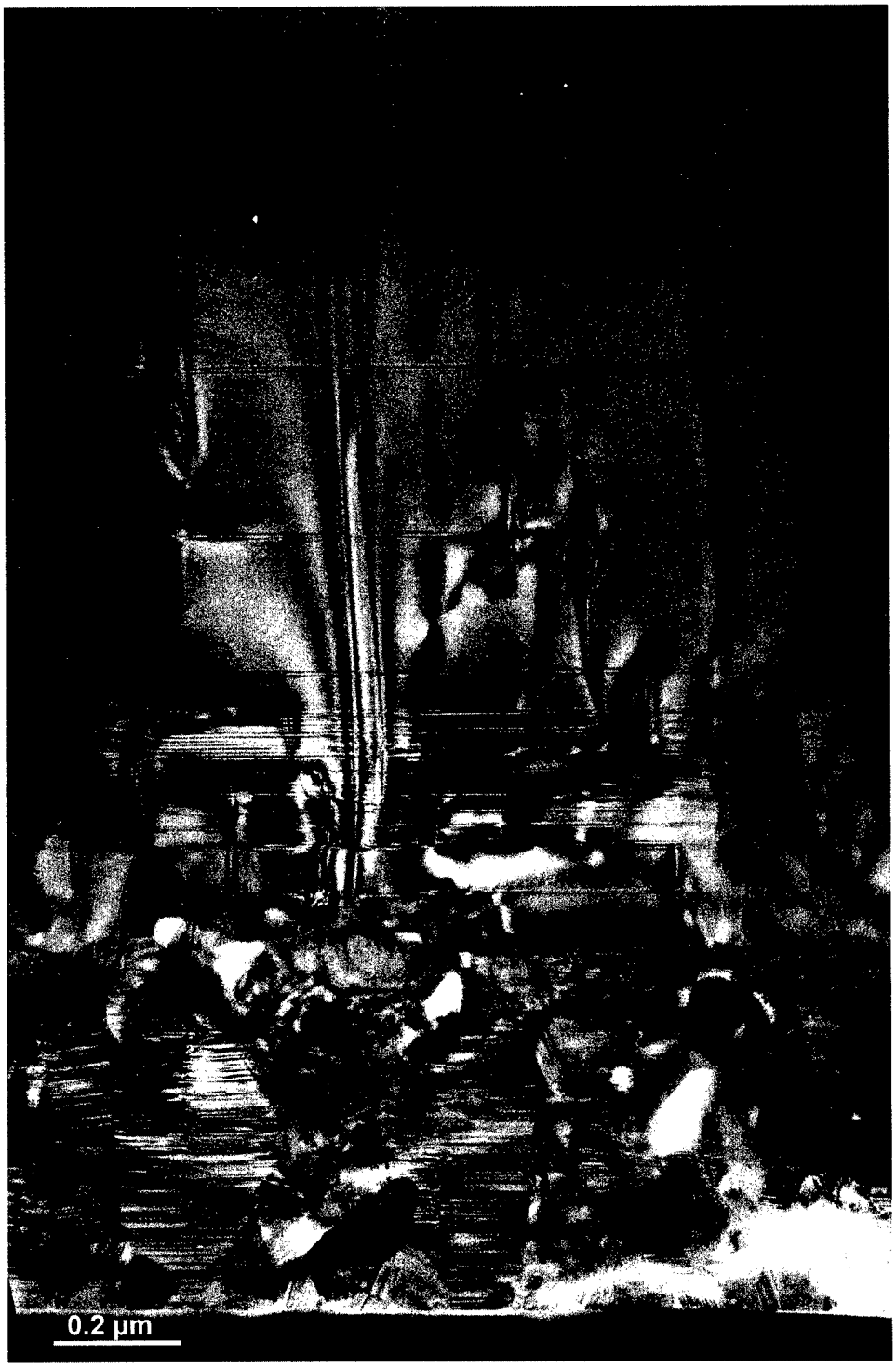

Figure 3. Cross-section TEM micrograph of HVPE grown GaN on c-plane sapphire substrates.

B. Development of Thick GaN Films by LEO-HVPE

The development of thick GaN films by the LEO-HVPE method is going to be used for the fabrication of detectors as schematically illustrated in Figure 4. In this method the (0001) sapphire substrate was coated first with a GaN film by the MBE method. Subsequently, ~100 nm silicon dioxide (SiO_2) was deposited by e-beam evaporation. Then stripes were lithographically patterned oriented in the GaN [1-100] or [11-20] by placing them perpendicular or parallel to the sapphire substrate flat. As schematically illustrated, the GaN in the window regions is highly defective and thus detectors have to be fabricated in the wings of the stripes.

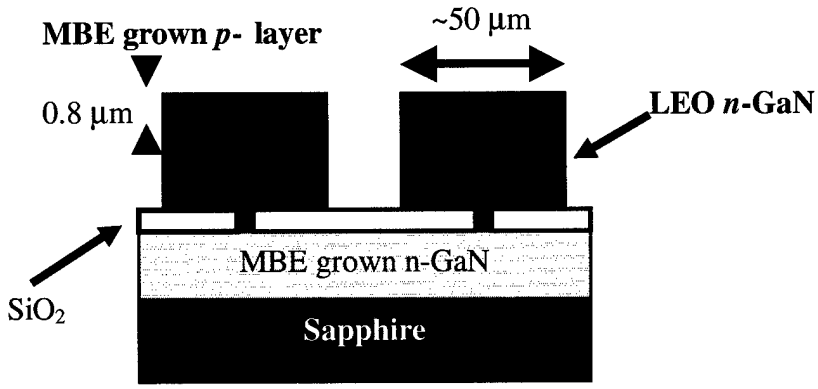

Figure 4. Schematic of a homoepitaxially grown pn junction on an HVPE-ELO GaN template.

The LEO-HVPE method was developed to lead to GaN stripes as wide as100 microns. This was possible because of the high growth rate obtained by the HVPE method (100 μm/hr). The threading dislocation density in these films was measured by transmission electron microscopy (TEM) to be about 10^6 cm^{-2} [2]. Figure 5 shows an optical microscope photograph of a 100 μm wide HVPE-grown LEO GaN.

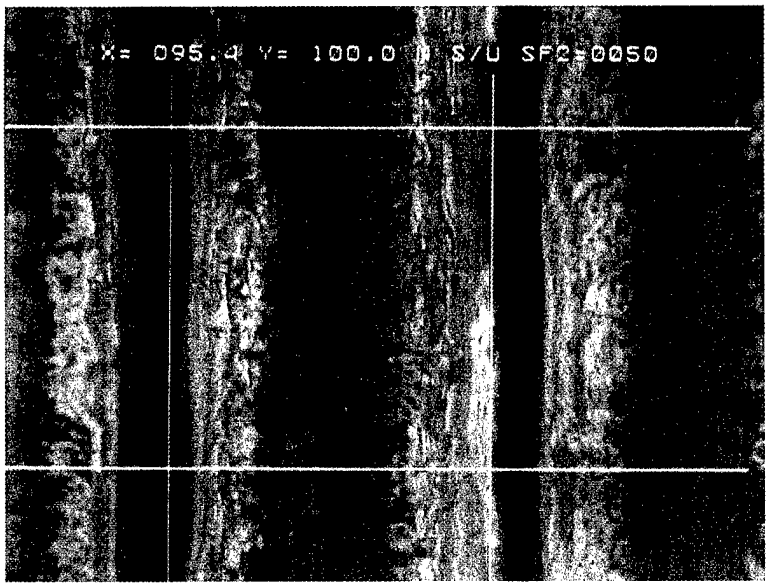

Figure 5. Optical microscope photo of a 100 μm wide ELO GaN bar

2.2. Growth and Doping of $Al_xGa_{1-x}N$ Alloys

The development of devices such as detectors operating at wavelengths shorter than 280 nm requires the development of the growth and doping of $Al_xGa_{1-x}N$ alloys with an AlN mole fraction greater than 40%. Presently, little work has been reported in the literature on the quality and doping of these materials using either the MOCVD or MBE techniques. It has generally been found that the n-type doping of these materials using silane by MOCVD is difficult.

Korakakis et al studied the doping of $Al_xGa_{1-x}N$ alloys grown by ECR- assisted MBE with AlN mole fractions < 25% [3]. The authors found that the dopant level of Si became progressively deeper within the gap with increasing AlN mole fraction. The Si dopant level was found by temperature dependent Hall effect measurements to be 17 meV for GaN and 54 meV for $Al_{0.18}Ga_{0.82}N$. In contrast, Polyakov *et al.* [4] found the Si level in a 40% alloy grown by MOCVD to be 50 meV and determined the upper limit for a 60% alloy to be only 90 meV. Consistent with other groups, the authors also found that the free electron concentration of $Al_xGa_{1-x}N$ alloys decreased with increasing Al

composition with a sharp drop off occurring for a 60% composition. Although these two studies need to be reconciled quantitatively, the trend of the Si donor becoming deeper with the AlN mole fraction is qualitatively consistent with the effective mass theory.

In the following we discuss the growth and doping of AlGaN alloys with high concentration Al. In addition to the doping studies, we have also addressed the issue of nucleation and propagation of cracks in AlGaN alloys with high Al concentration.

A. Development of interlayer buffer layers during growth of AlGaN alloys by MBE

The lack of thick bulk III-Nitride substrates has led various groups to explore different nucleation steps to reduce the dislocation density in heteroepitaxial grown III-Nitride films. Amano and coworkers have developed a method using MOCVD that involves the addition of a several thin low temperature buffer layers that are interspersed between high temperature layers. These layers, referred to as interlayers, consisted of GaN or AlN were grown at 500 °C.

Amano *et al.* [5] studied the stress in GaN films grown on either GaN or AlN interlayers using XRD measurements at room temperature. The authors discovered that the tensile stress in the GaN films grown on low temperature GaN interlayers increased with an increasing number of interlayers before saturating at 1 GPa for films with 3 or more GaN interlayers. The saturation in the tensile stress was attributed to cracks that developed in these films. In contrast, GaN films grown on AlN interlayers were compressively strained at room temperature and the stress was found to be nearly independent of the number of interlayers. No cracks developed in the films grown on an AlN interlayer. The authors note that TEM studies show that the free surface of GaN films grown using either interlayer showed a reduction in dislocation density.

Kamiyama *et al.* [6] have investigated the growth of $Al_xGa_{1-x}N$ films on these interlayers. They observed that the FWHM of the x-ray rocking curve as well as surface morphology of the $Al_xGa_{1-x}N$ films degrade with increasing AlN mole when they were deposited on a single low temperature AlN buffer layer. In contrast, the FWHM of the x-ray rocking curve of $Al_xGa_{1-x}N$ films deposited on a LT AlN interlayer separated by a 1μm thick GaN layer were found to be independent of AlN mole fraction. Films grown directly on an AlN buffer layer as well as on an AlN interlayer were studied by TEM. The authors found that the density of dislocations in films grown directly on AlN buffer layers increases exponentially with AlN mole fraction. In contrast, the dislocation density of similar films grown on an AlN interlayer buffer saturates at $\sim 5 \times 10^9$ cm^{-2} for AlN mole fraction > 20%. The improvement in the crystalline quality of the $Al_xGa_{1-x}N$ layers was attributed to an enhancement in the 2D mode of growth by the LT AlN interlayer.

The films investigated in our work were deposited on c-plane sapphire using two 5 nm thick AlN interlayers separated by 75 nm thick unintentionally doped $Al_{0.4}Ga_{0.6}N$ layers. Finally a 1μm thick epitaxial n- $Al_{0.4}Ga_{0.6}N$ layer was deposited using the same growth conditions employed for the spacer layer except for the introduction of Si. The

$Al_xGa_{1-x}N$ layers were grown at 750 °C using an Al flux of $1.15x10^{-7}$ Torr, and a Ga flux of $3.5x10^{-7}$ Torr. The AlN interlayers were deposited using the same conditions employed for the buffer layer (Al flux = $1.15x10^{-7}$ Torr, power = 100W). The AlN interlayers were deposited at a substrate temperature between 500-750 °C. Table 1 shows a summary of the growth conditions of the investigated AlGaN films with interlayers and Figure 6 shows a schematic of the deposited interlayer nucleation scheme.

Table 1. Summary of growth conditions for AlGaN films deposited on AlN interlayer buffers

Sample	Interlayer Temperature (°C)	Ga Flux Al Flux	Si Temperature (°C)
1063	750	4.00E-7 8.48E-8	1150
1066	750	3.5E-7 1.15E-7	1160
1072	750	3.5E-7 1.15E-7	1120
1073	600	3.5E-7 1.15E-7	1120
1074	550	3.5E-7 1.15E-7	1060
1075	500	3.5E-7 1.15E-7	1090

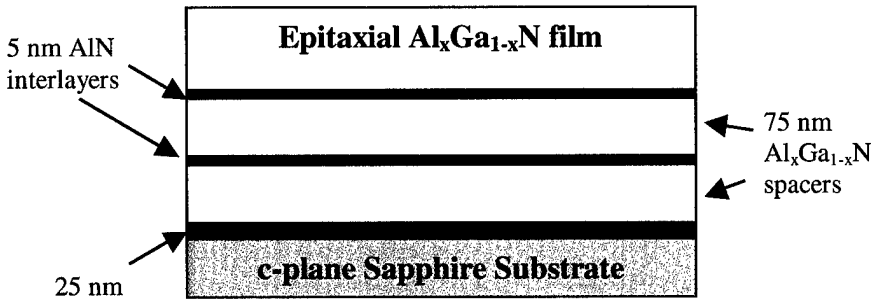

Figure 6. Schematic of AlN interlayer buffer using $Al_xGa_{1-x}N$ spacer layers.

Figure 7 shows the transmission spectra for two samples grown with LT AlN interlayer and two samples grown with a HT AlN interlayer. All the films grown on the interlayer buffers are observed to have a sharp band edge absorption.

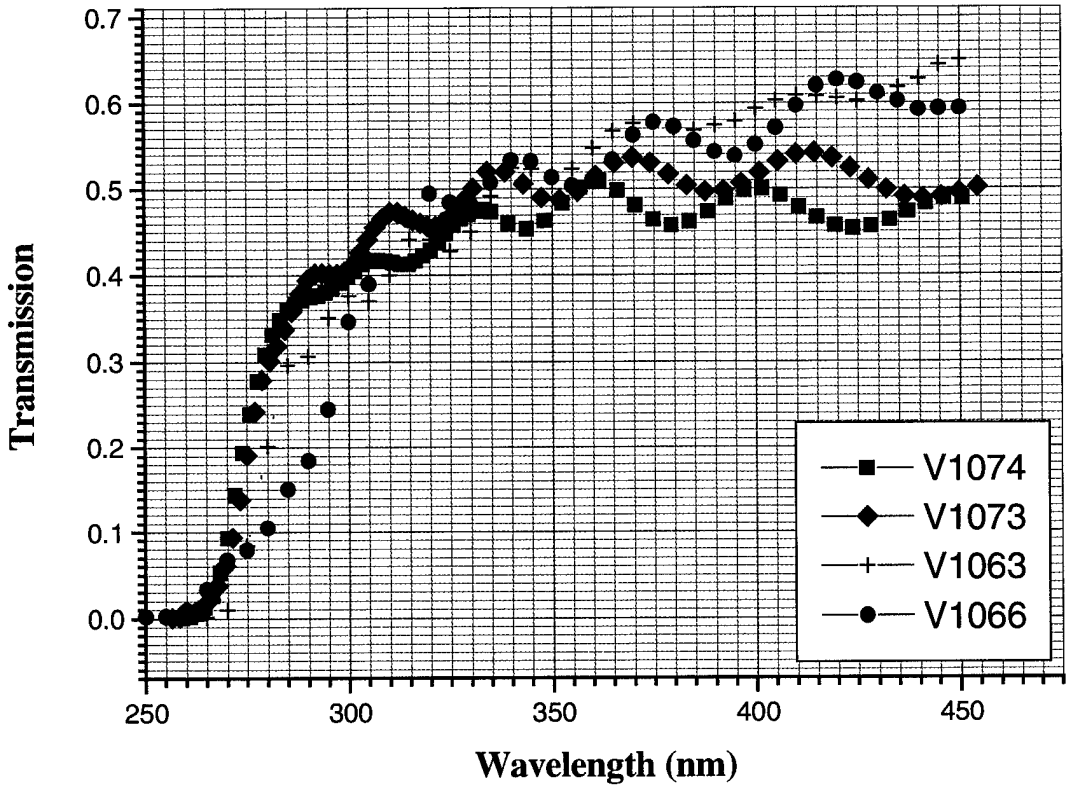

Figure 7. Transmission spectra of $Al_xGa_{1-x}N$ films deposited on an AlN interlayer buffer

B. Doping of AlGaN alloys

The doping of $Al_xGa_{1-x}N$ n-type has not been reported extensively to date. The free carrier concentration of the samples plotted as a function of reciprocal Si cell temperature is shown in Figure 8. It is clearly seen in Figure 8 that the free carrier concentration in the AlGaN films can be varied as a function of Si cell temperature. We have been able to doped films with Al content as high as 50% (V1068) degenerately to 10^{19} cm^{-3}.

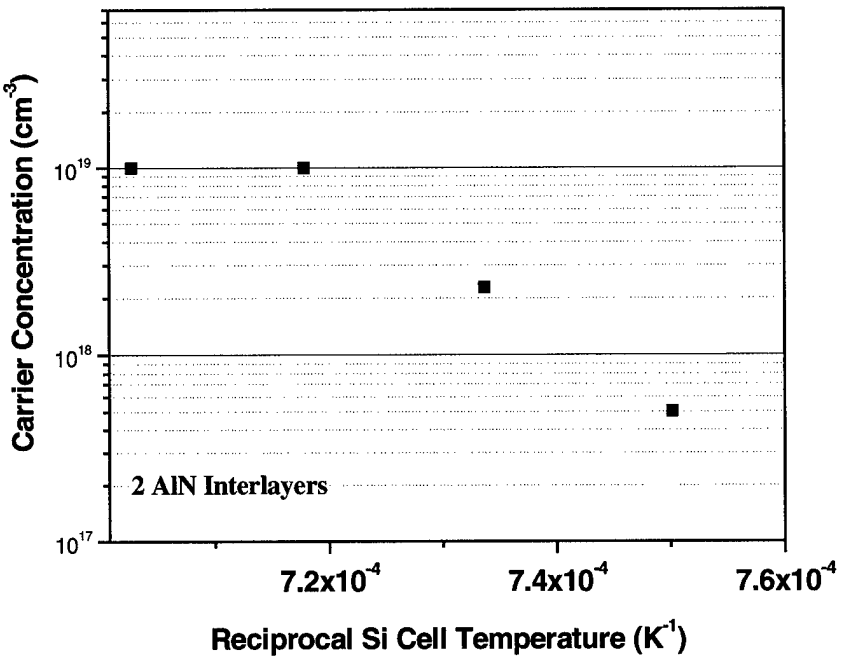

Figure 8. Carrier concentration vs. $1000/T_{Si}$ for 40% $Al_xGa_{1-x}N$ alloys

C. Effect of interlayers on strain control of AlGaN films

Films that were grown with and without the interlayer buffers were studied by SEM to determine what effects these multiple buffers have on the cracking of the film. Figure 9 shows a typical SEM micrograph (left) of an $Al_{0.4}Ga_{0.6}N$ film deposited using either a low temperature or a high temperature AlN interlayers. It is observed that the formation of cracks in these films are suppressed. In contrast the SEM micrograph of the film deposited using a single AlN buffer layer (right) reveals a large amount of cracking in these films. We believe that the cracking observed in the films deposited without an AlN interlayers is due to tensile stress on the film as a result of the difference in thermal expansion coefficients between the sapphire substrate and the $Al_{0.4}Ga_{0.6}N$ film.

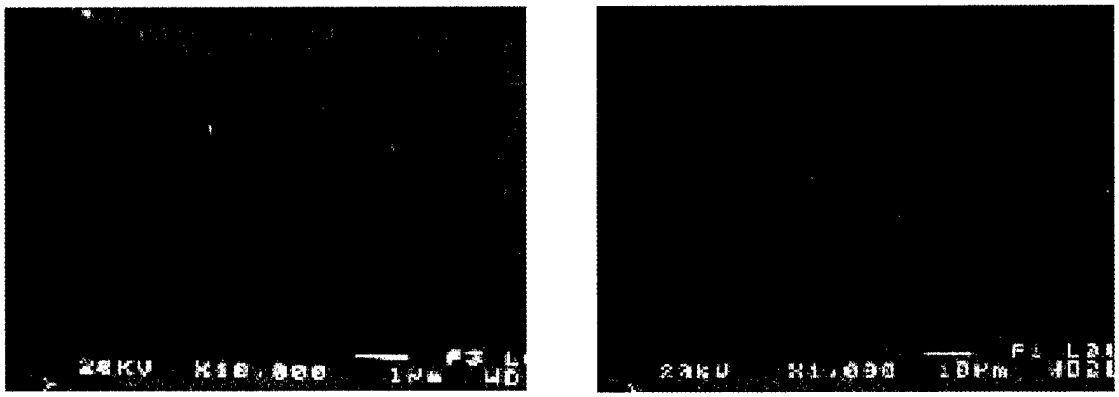

with interlayer without interlayer

Figure 9. SEM micrographs of $Al_xGa_{1-x}N$ films grown with and without an AlN interlayer

2.3. Design of a Solar Blind UV Detrector

The design of the Solar Blind Detector (SBD) is based on the solar transmission spectra shown in Figure 10. It is evident from the plot that at low altitudes there is a very large transmission across the spectrum with the exception of the wavelengths between 240- 280 nm. A detector that is sensitive in this window would see very low ambient radiation and therefore would be highly sensitive to sources of radiation at these wavelengths.

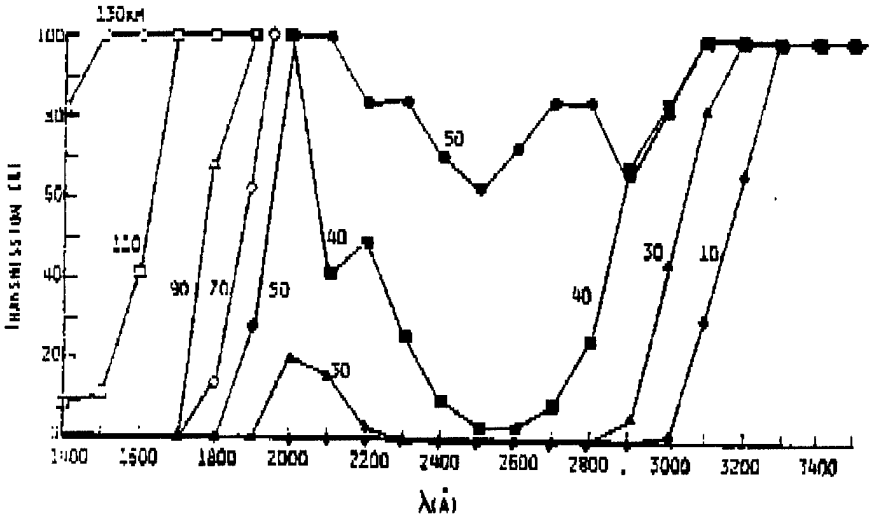

Figure 10. Solar transmission spectrum at various altitudes

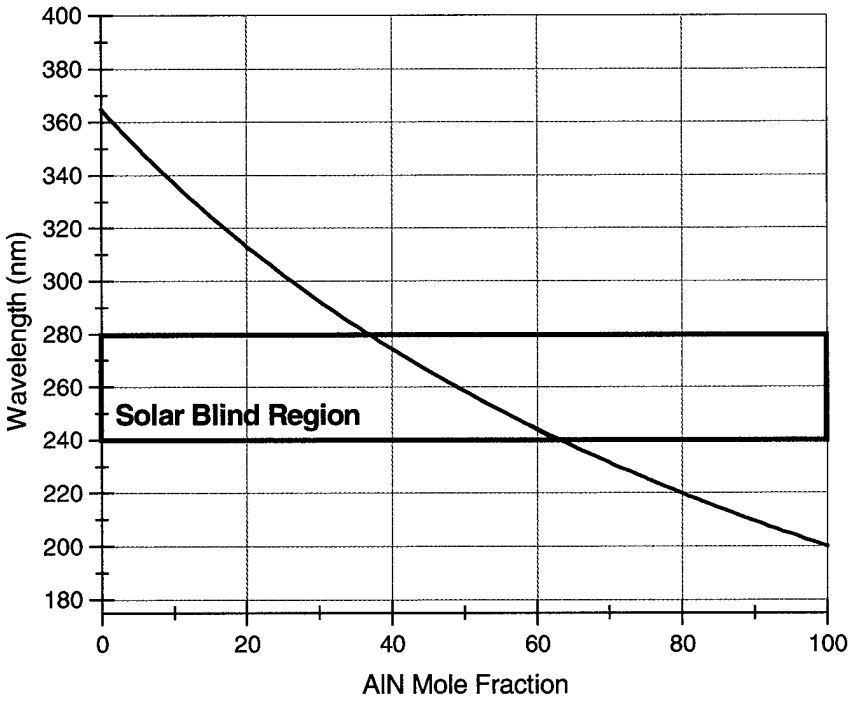

Figure 11. $Al_xGa_{1-x}N$ absorption edge vs. AlN mole fraction.

The absorption edge of $Al_xGa_{1-x}N$ can be tuned for wavelengths between 200-365 nm by adjusting the AlN mole fraction in the alloy as shown in Figure 11. The absorption edge of the alloy is determined using Vegard's Law and assuming no bowing. Actual experimental data suggests that the bowing parameter is non-zero and that it can be dependent on growth conditions. Based on this approximation, a 62% AlN mole fraction alloy would have an absorption edge at 240 nm and could be used as the short wavelength filter. A 35% AlN mole fraction alloy would have an absorption edge at 280 nm and could be used as the absorber region where the detector would collect light. Since this alloy will be transparent for wavelengths longer than 280 nm, filters that are generally employed to attenuate these wavelengths for Si-UV detectors are not required. Figure 12 shows two basic device structures for a p-i-n based SBD.

A schematic for a back-illuminated a p-i-n diode, based on either a homo- or a hetero- junction, is shown in Fig 12(A). Light impinges the detector from the substrate and is filtered by the high AlN mole fraction n^+ layer. Light with wavelengths between the 240-280 nm is then collected in the n^- - $Al_xGa_{1-x}N$ layer. Employing a heterojunction will minimize the difficulty in depositing a high quality p-layer while collection of carriers generated in the p-layer should be minimal due to the very short minority diffusion lengths in p-GaN. This configuration is convenient for the fabrication of arrays where the device may be flip-chip bonded to a Si read-out system.

Another configuration, shown in Fig 12(B), may be employed for creating a front-illuminated device. The principal remains the same, however the top metal contact must be made either transparent or have a grid geometry to allow for the collection of light. This is due to the large sheet resistances in these layers that can cause inhomogeneous current spreading and premature breakdown.

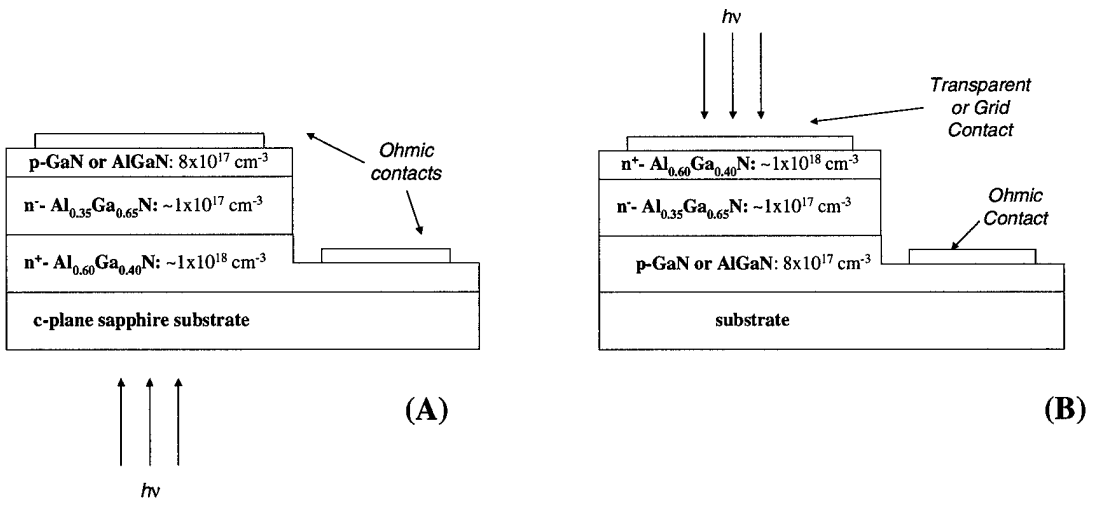

Figure 12. Structure of a solar-blind photodetectors for (A) back- and (B) front-illumination.

One difficulty in fabricating this structure is that damage to the p-GaN material during the dry etch process causes type inversion to occur at its surface. This could be avoided by employing a configuration similar to Fig 12(A), but employing a ~60% AlN mole fraction p- $Al_xGa_{1-x}N$ alloy. This configuration however is presently impractical because of the difficulty in doping these alloys p-type.

2.4. Device Design/Photomask Development

The fabrication of devices requires the creation of a photolithographic mask set. The set can consist of a number or patterns that are ultimately to be defined on the sample. A separate pattern is generally required for each level or step of the fabrication process. For example, the creation of a photoconductive detector requires the deposition of a single metal stack and can be done with one lithographic step to determine the pattern of the device. Therefore this would require one mask pattern. However, if you wanted to isolate your devices by etching away or ion implanting the material between the devices, then a second step would be required to define this area. This would require a second pattern and another mask and both masks would have to include appropriate alignment marks to facilitate the proper alignment of these two patterns. In this section, we discuss the design and use of the photomask set developed for this work and the devices and test structures that have been incorporated into it.

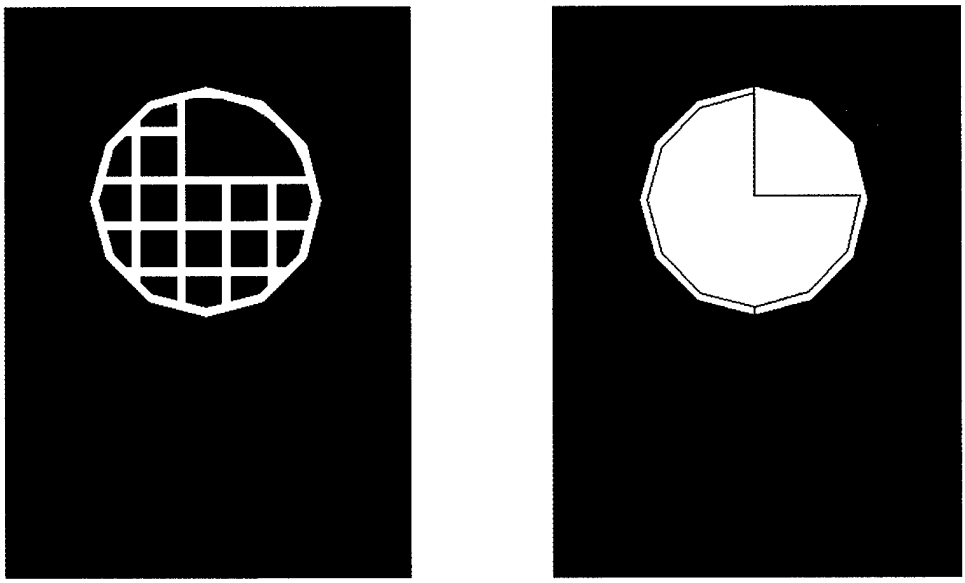

Figure 13. Two different front illuminated detector structures. Device A employs a p-ohmic grid. Device B employs a thick p-ohmic ring and a thin transparent contact.

For a front-illuminated p-i-n photodetector mask set, we developed a three level mask set for 1) etching a mesa to expose the bottom n^+ -layer, 2) depositing the n^+ -ohmic

contact and 3) depositing the p- ohmic contact. Since p-type GaN is generally highly resistive, it is necessary to fully metalize the top p-contact to insure proper current spreading. As a result, three different patterns have been made for this metal. The first is a metal grid that allows illumination through the windows in the grid. The other two levels work in concert as a thick metal contact for probing and a very thin optically transparent contact. These two types of devices are shown in Figure 13. In addition, a level has been added to insert an oxide isolation layer for floating the p-ohmic pad off the n-layer to maximize the optical area of the device.

The mask set device die designed for p-i-n detectors is shown in Figure 14. The three main devices that are included in the mask design are: 1) 300 μm circular diodes, 2) 1x1 mm square diodes and 3) 8x8 pixel, front-illuminated photodetector arrays. he circular diodes were designed with two configurations, one employing an oxide-layer to float the top contact layer and maximize the optical area of the device and another simpler diode that accommodates the top contact on the mesa surface. A number of test structures were incorporated into the mask set to study various aspects of the semiconductor material or device. Table 2 provides a concise list of the structures included.

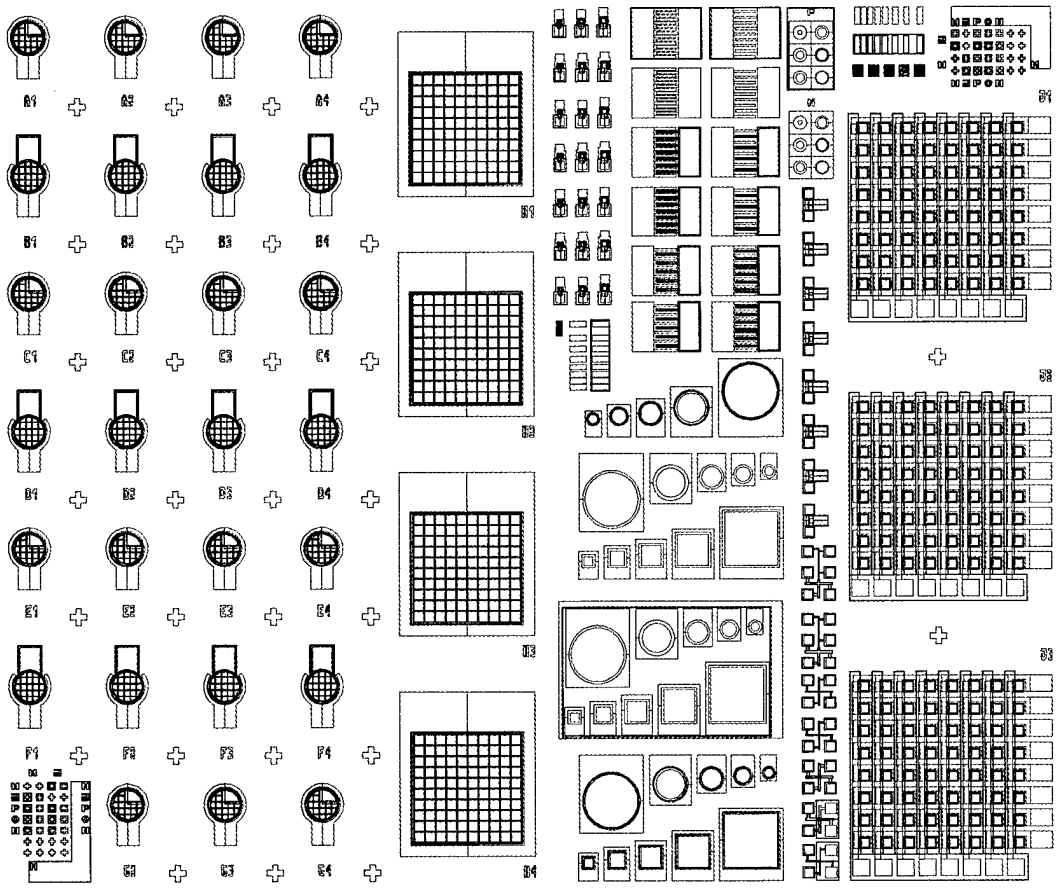

Figure 14. Designed p-i-n mask set device die.

Table 2. Summary of test structures incorporated into photodetector mask set.

Structure	Purpose	Dimensions
Rectangular TLM	Determine resistance of contacts to top and bottom material	Spacings off 5,10,15,20,40,50,75 μm
Variable Area Circular Diodes	Determine the dependence of leakage currents on area vs. perimeter	100,150,200,300,500 μm diameter
Variable Area Square Diodes	Determine the dependence of leakage currents on area vs. perimeter	100,150,200,300,500 μm side length
Variable Area Schottky Diodes	Determine the doping level of top and bottom layers	100,150,200,300,500 μm
Variable Area MOS Capacitors	Determine the breakdown and leakage of the pad oxide layer	100,150,200,300,500 μm diameter
Kelvin Resistors	Determine the sheet resistance of the top material	Channel widths varying from 6,10,20 μm
Small Area Diodes	Defect minimized devices	30 x 30 μm^2, 40 x 40 μm^2, 50 x 50 μm^2

The critical structures incorporated for studying the nature of the reverse leakage currents in these devices are the variable area circular and rectangular diodes. By investigating the reverse leakage current dependence on the area and perimeter of the variable size diodes it was thought that the nature of the leakage current could be determined. If the current scaled linearly with the area of the diodes, this would suggest that the leakage was related to bulk material phenomena. In contrast, if the current scaled linearly with device perimeter then that would suggest that the leakage was related to the mesa sidewall.

2.5. Device Configurations Investigated

2.5.1 Schottky-Diode Devices

An ideal Schottky diode is fabricated on n-type semiconductor material by depositing a metal having a work function (Φ_m) greater than the electron-affinity (χ_s) of the semiconductor. These devices are faster than p-i-n junction based devices because they do not suffer from minority carrier storage. However, these diodes tend to have larger reverse-bias leakage current than p-n junction diodes due to thermionic emission of majority carriers over the Schottky barrier. A number of n^+/n^- -GaN and -$Al_xGa_{1-x}N$ based vertical Schottky diodes have been fabricated in this work. The GaN based devices were grown both homo- and heteroepitaxially. $Al_xGa_{1-x}N$ based structures were deposited using the interlayer nucleation technique.

A. Homoepitaxially and Heteroepitaxially Grown GaN Schottky Diodes

Homoepitaxy is a promising method for improving the quality of MBE grown GaN detectors. We studied the impact of homoepitaxial growth on GaN Schottky photodetectors by comparing devices grown on GaN templates grown by hydride vapor phase epitaxy with similar devices grown heteroepitaxially on c-plane sapphire using the three-step growth method consisting of nitridation of the substrate, low –temperature GaN or AlN buffer and high temperature film. The heteroepitaxially grown diodes consisted of a 2.25 μm thick n^+ -GaN (doping level of about $5x10^{18}$ cm^{-3}) followed by a similar n-GaN layer doped at ~$5x10^{16}$ cm^{-3}. A similar device was deposited homoepitaxially on 5 –6 μm thick GaN templates grown by the HVPE method. The structure of both devices is shown in Figure 15.

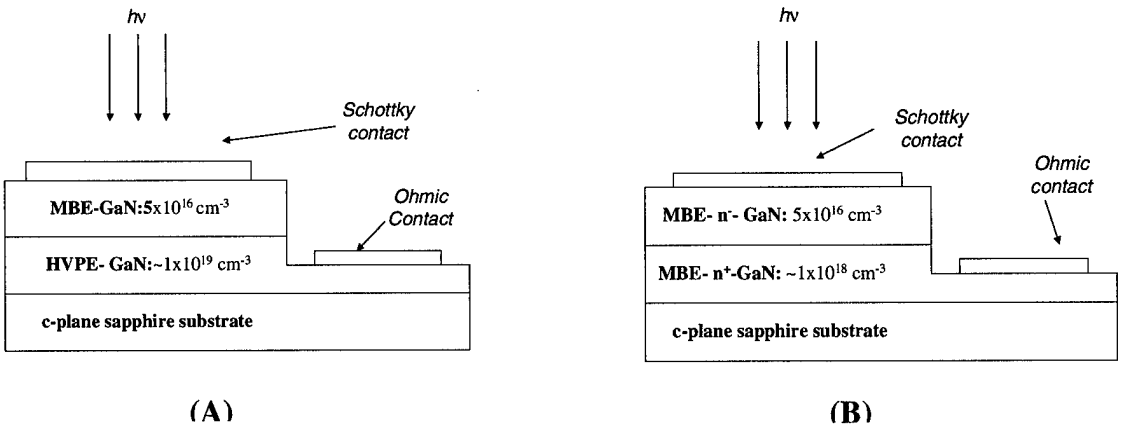

Figure 15. Homoepitaxial and Heteroepitaxially grown GaN Schottky diode structures.

Typical I-V characteristics for the two types of Schottky diodes are shown in Figure 16. Both the homo- and heteroepitaxially grown devices showed nearly ideal behavior over 4 decades in current, and had an ideality factor between 1.2-1.4. The reverse saturation current for the homoepitaxially and heteroepitaxially grown diodes are 1.4 and 1.2×10^{-9} A/cm^2 respectively. The C-V measurements demonstrate that the n^- GaN layer in both types of Schottky diodes has a free donor carrier concentration of 6-9×10^{16} cm^{-3} and the barrier height of both diodes were between 0.9-1 V (see Figure 17).

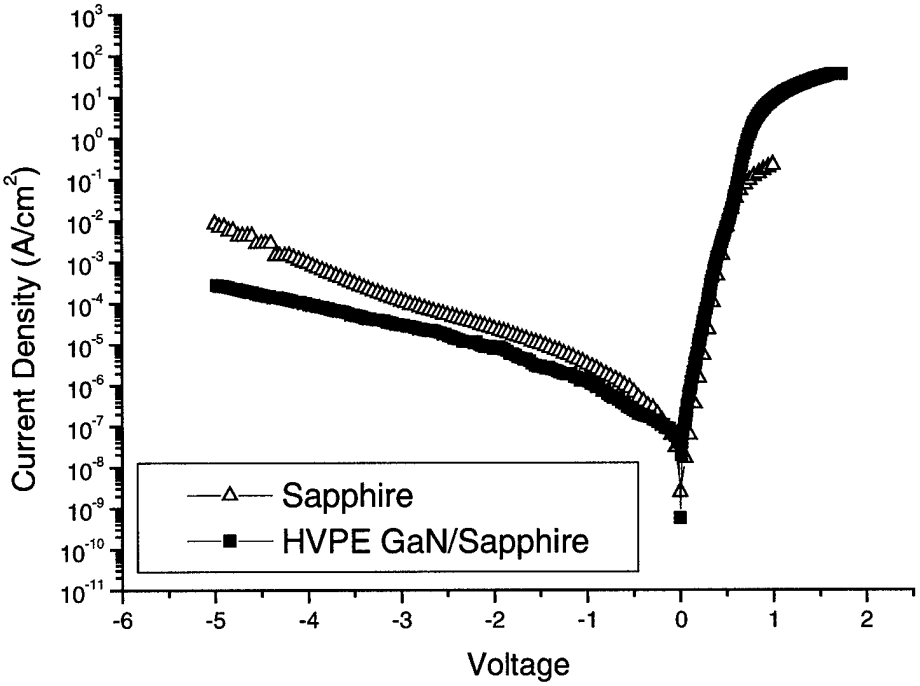

Figure 16. I-V characteristics of homo- and heteroepitaxially grown GaN based Schottky diodes.

The 300 μm diameter diode fabricated on HVPE-GaN has a leakage current density of 2.75×10^{-4} A/cm^2 at –5V reverse bias that is over 1 order of magnitude lower than the heteroepitaxially grown one. This improvement is attributed to the reduction of threading defects in the homoepitaxially grown device.

The forward bias characteristics of the diodes are compared in Figure 18, employing a modification to the ideal diode equation that accounts for the voltage drop across the parasitic series resistance of the device:

$$I = I_0 e^{\frac{q(V-IR_S)}{nkT}}$$

where I is the diode current, V is the applied voltage and R_s is the series resistance of the diode.

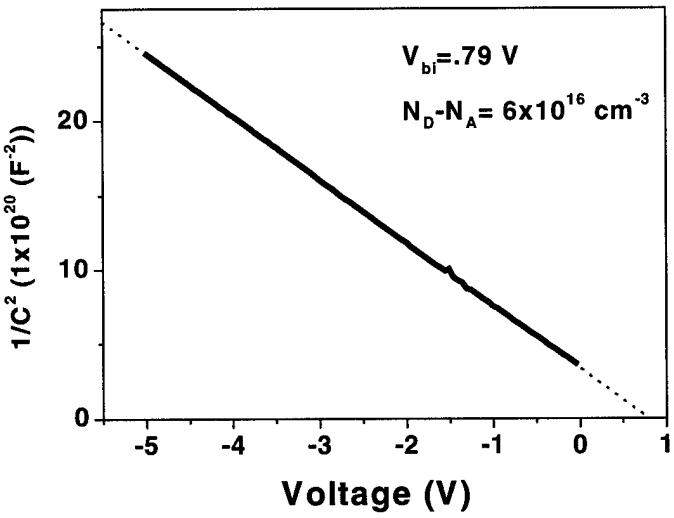

Figure 17. C-V characteristics of the homoepitaxially grown Schottky diode.

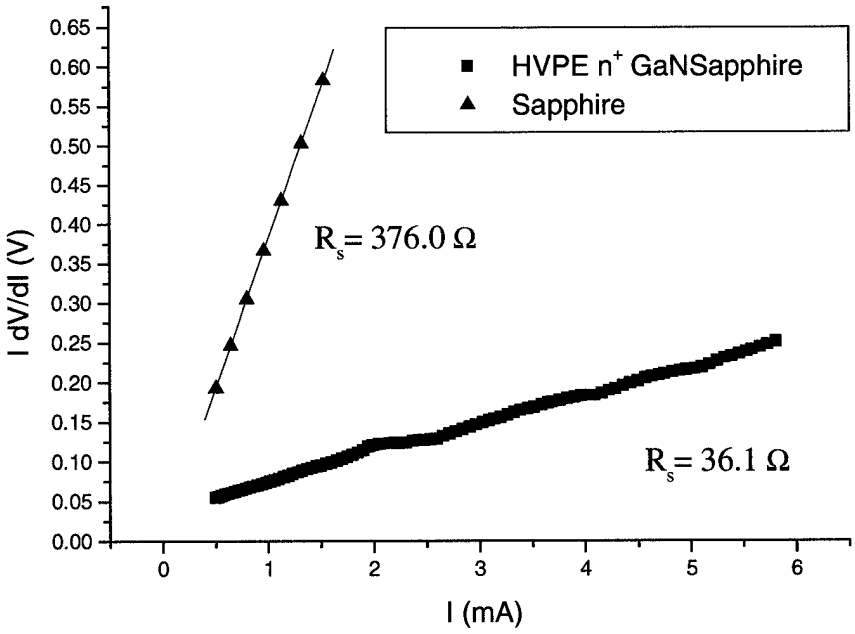

Figure 18. Study of the forward series resistance in GaN based Schottky diodes.

Then, the series resistance of the device may be determined from the slope of the linear I dV/dI vs. I plot. It was observed that the heteroepitaxially grown device had ~ 1 order or magnitude higher series resistance than the homoepitaxially grown device. We believe that the larger forward resistance of the heteroepitaxial device has two origins. One is due to the larger series and contact resistance of the n^+ -GaN MBE-grown layer. The second contribution comes from the reduction of the active area in the n^- GaN layer due to the higher concentration of dislocations in this device. Specifically, as demonstrated by Misra and coworkers [7], the transport in vertical GaN devices does not suffer from scattering by charged dislocations. However, the series resistance of the device is expected to increase as the density of dislocations increases due to the reduction of the active area for conduction. This results from depletion around each dislocation. A quantitative description of the dependence of series resistance in the forward direction requires an accurate determination of the dislocation density in the sample.

Figure 19 shows the spectral dependence of the responsivity measured for the two vertical Schottky barriers. The spectral response of the heteroepitaxially grown device

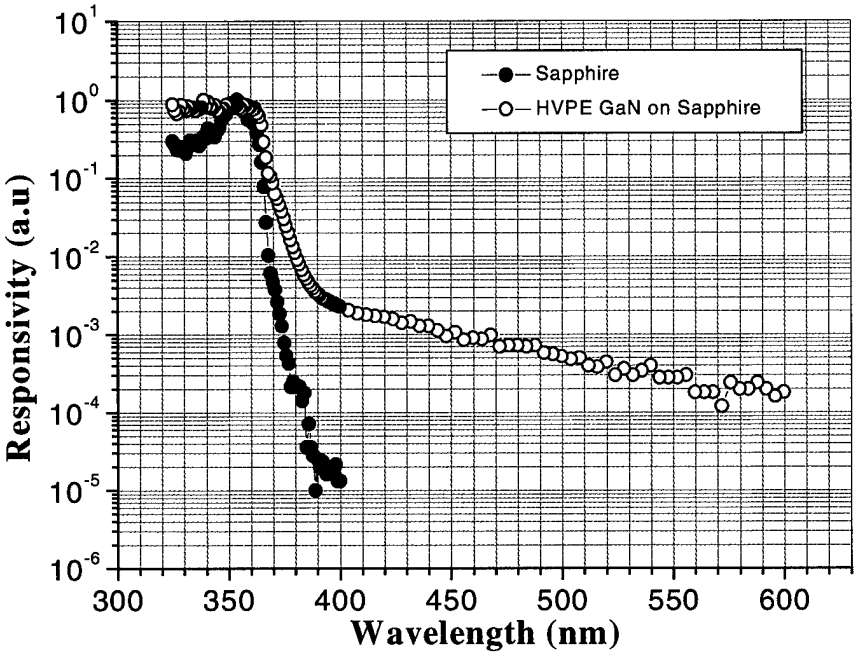

Figure 19. Spectral response of GaN based vertical Schottky diodes.

was measured at –4 V bias and the responsivity of this device at 325 nm was measured to be 0.05 A/W corresponding to an internal quantum efficiency (η) of 25%. A peak response of 0.18 A/W (η= 70%) was found to occurs at 355 nm. This spectral response shows a sharp transition at the gap of the semiconductor of about 5 orders of magnitude visible light rejection. This is one of the highest values reported in the literature.

The responsivity of the homoepitaxially-grown device was similarly measured to be .27 A/W at 325 nm and –3.5V bias. To within the accuracy of the measurement (~ 20%) these devices show nearly ideal response between 325 and 355 nm. However, a visible rejection of only 2.5 orders of magnitude is observed for this device between band gap and 400 nm followed by a long exponential drop that extends to about the middle of the gap of the semiconductor. A possible explanation for the exponential tail observed in this device is due to light absorption and collection from the thick HVPE n^+ -GaN\sapphire substrate. It is possible that sub-band gap light can generate carriers in \ the heavily doped (~$1x10^{19}$ cm^{-3}) HVPE n^+ -GaN by optical transitions from band tails in the valence band (due to potential fluctuations) to the conduction band. Pankove and coworkers have observed such band tails in GaN previously [8].

It is worth noting that the electrons generated by transitions from the valence band tail to the conduction band occur outside of the depletion region in the vertical Schottky diode. However, these electrons are collected because their diffusion length is very long. Specifically, the $\mu\tau$ product calculated from photoconductivity gain measurements for n-GaN films Si doped at $1x10^{18}$ cm^{-3} was found to be about 10^{-3}-10^{-2} cm^2/V [9]. From the Einstein relation, a diffusion length of ~50 μm is calculated from this $\mu\tau$ product. Since the ohmic contact to the device is made to the HVPE n^+-GaN film, carriers generated there can be collected very efficiently.

The implication of this result is that diodes grown directly on the HVPE n^+-GaN\sapphire substrates will always have a poor visible to UV rejection ratio because of carrier generation and collection from the thick n^+ GaN substrate. Therefore, these substrates need to be more lightly doped (~ 10^{17} cm^{-3}).

B. $Al_xGa_{1-x}N$ based Schottky devices

The work on Schottky barrier based detectors was extended deeper into the UV by fabricating vertical detectors using $Al_xGa_{1-x}N$ alloys. The device structure consisted of a 1.5-micron thick 55% AlN mole fraction n^+- $Al_xGa_{1-x}N$ alloy deposited on 2 AlN/AlGaN interlayers as schematically shown in Figure 20. Subsequently, a 200 nm thick n^- - AlGaN alloys having 35% AlN mole fraction was deposited. When back-illuminated absorption from the high AlN mole fraction layer should make this diode solar-blind. However, this device may also be front-illuminated through the Schottky grid contact. This has the advantage that the spectral response can be investigated independent of the high AlN mole fraction window layer and therefore the impact of this layer on device performance may be studied.

The IV characteristics of this device were measured on the unfabricated wafer (see Figure 21). The ohmic contact was formed by an In dot that was soldered to the bottom n^+- $Al_xGa_{1-x}N$ layer that was exposed by scratching the wafer with a diamond scribe. The Schottky contact was formed using a Au wire. A zero-bias differential resistance of 10^{11} Ω was measured from the wafer-level IV characteristics. Further

reduction in the reverse leakage current should be possible by optimizing the interlayer buffer technique.

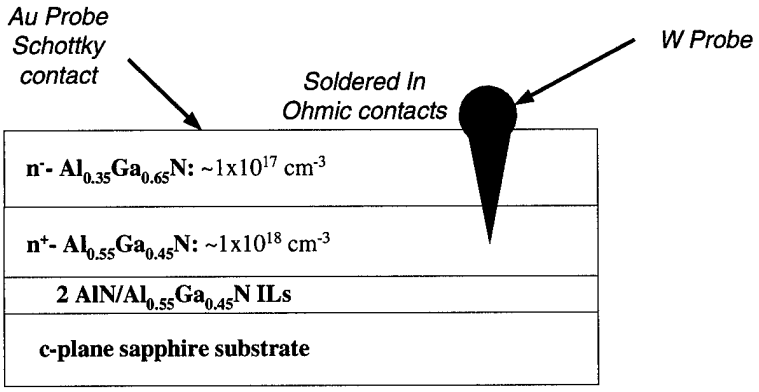

Figure 20. Schematic of wafer level I-V measurement of a AlGaN Schottky diode.

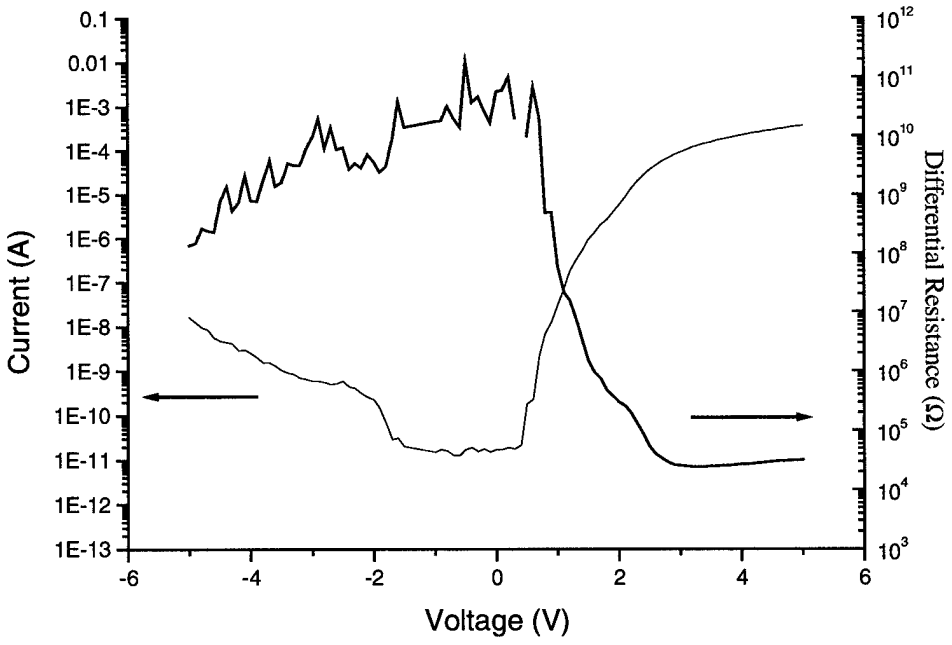

Figure 21. Wafer level IV characteristics of a AlGaN Schottky diode.

2.5.2 GaN p-n junction diodes grown on HVPE GaN Templates

Homoepitaxially grown p-n junctions have been fabricated by depositing a Mg-doped GaN layer on a HVPE grown GaN template. The MBE grown p-GaN layers were between 300-500 nm thick and had a free hole concentration of ~ $8x10^{17}$ cm^{-3}. Figure 21 shows the IV characteristics of a 300 μm diameter diode. A dark current of less than 10^{-11} A/cm^2 was measured at –2V bias for these devices. The dark current seen in these diodes is attributed to the leakage through the remaining dislocations in the film. The devices discussed in Figure 21 show more than an order of magnitude lower dark current than a corresponding device grown by MBE on sapphire substrates. Further improvements should be achieved with the use of thicker HVPE n-GaN films since the dislocation density in such films have been shown to decrease monotonically with film thickness [10].

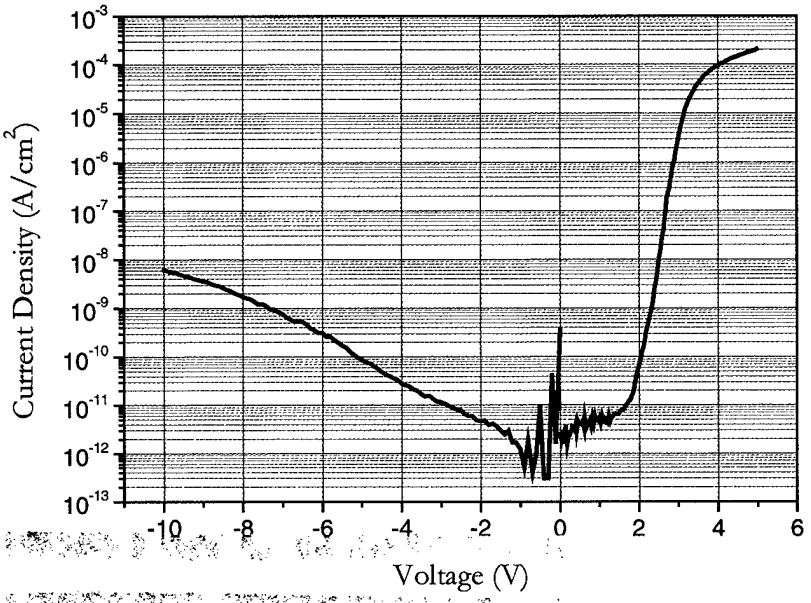

Figure 21. I-V Characteristics of a homoepitaxially grown pn junction.

To further investigate this hypothesis electron beam induced current (EBIC) studies were performed on these devices. For these measurements diodes with a 290 μm diameter ring contact was used which allows the electron beam to directly probe the p-GaN surface. The SEM and EBIC images of such a device are shown in Figure 22. The correspondence between the pits in the p-GaN layer shown in the SEM image and the leakage current in those areas in the EBIC image unambiguously correlates the leakage current under reverse bias with the number of dislocations in the material.

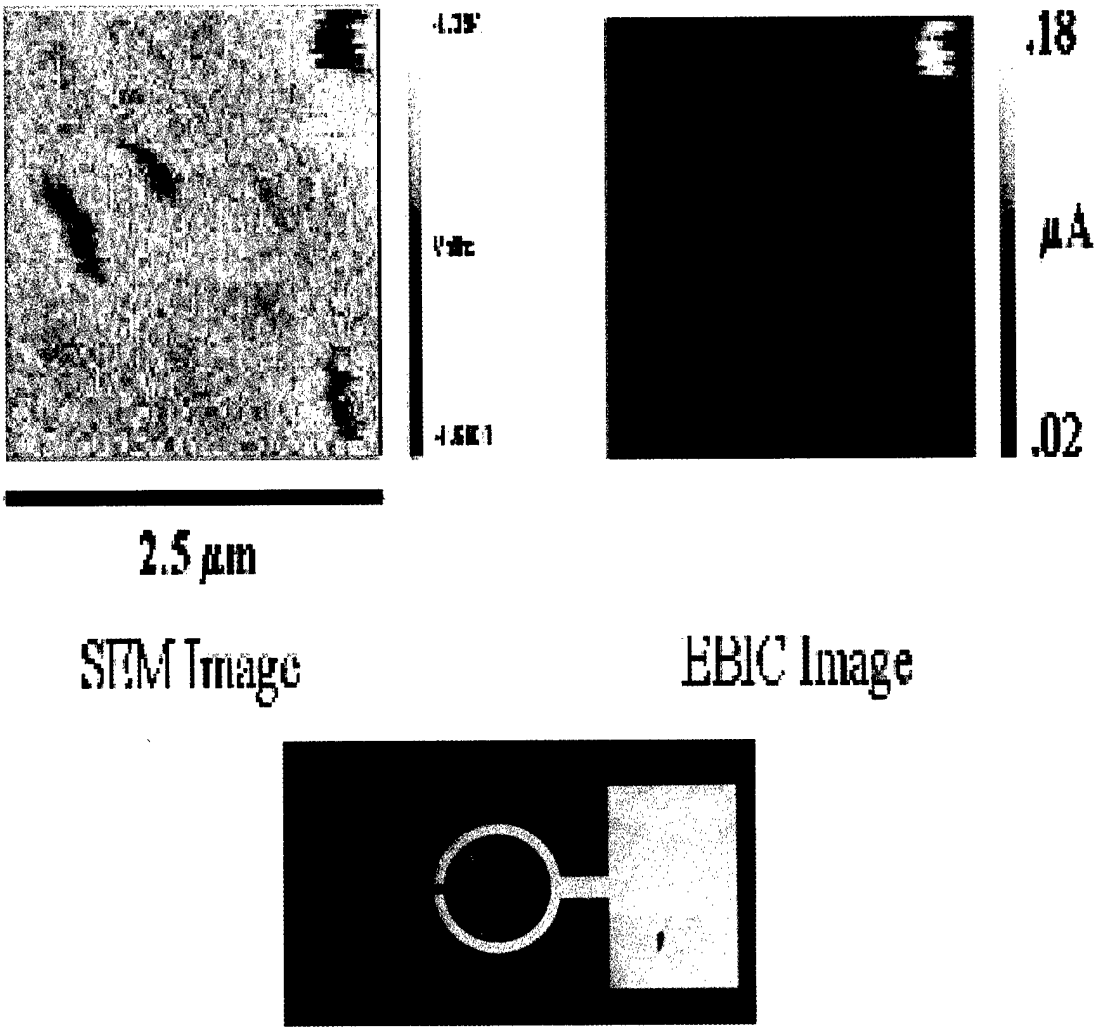

Figure 22. SEM and EBIC images of a fabricated GaN pn junction (bottom).

2.5.3. GaN *pn*-junctions grown on ELO GaN templates

A larger reduction in reverse leakage current should be possible by further reducing the number of dislocations in these materials One method to accomplish this is to growth the HVPE deposited GaN templates using the epitaxial lateral overgrowth (ELO) technique. This method consists of depositing SiO_2 stripes on either a GaN film or a bare sapphire substrate. These stripes are oriented in the GaN (1-100) or (1-120) direction by placing them perpendicular or parallel to the sapphire substrate flat. GaN grown in the window regions are generally highly defective, however the material that grows laterally over the SiO_2 mask regions have been found to have considerably lower density of

defects. A schematic of an ELO stripe is shown in Figure 4. It is clear that the best devices should be located solely in the laterally grown region of the material.

The precise alignment of the silicon dioxide stripes to the sapphire substrate is achieved using a special alignment key designed into the photomask plate that consists of a set of 5 μm wide bars spaced 45 μm apart (Figure 23). Angular alignment of the stripes with the substrate flat is accomplished by insuring that its flat does not break two adjacent bars in the alignment key. Using this technique stripes with widths of 10,30 and 50 μm and spacings of 2 μm have been defined by using standard lithography methods in silicon dioxide films deposited by e-beam evaporation from SiO_2 pellets in an oxygen ambient. The silicon dioxide mask has been patterned by wet etching in dilute BOE or by dry etching in the Plasmatherm RIE using CF_4.

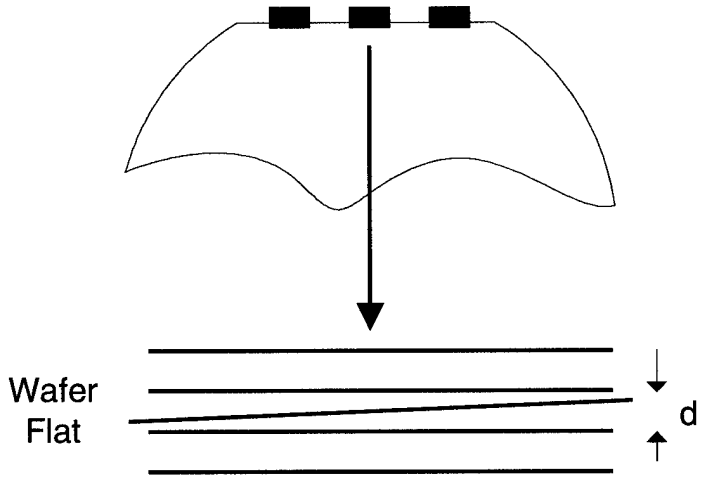

Figure 23. ELO mask set angular alignment key

Subsequently, GaN is regrown on the patterned substrate by the HVPE method. Growth initially begins vertically in the gaps between the silicon dioxide bars and then extends laterally over the silicon dioxide. The laterally grown material (sometimes referred to as the "wing" region) has been found to have dislocation densities less than 10^7 cm^{-2} [2]. Figure 5 shows an optical microscope photograph a 100 μm wide HVPE grown ELO-GaN bar deposited on an ~1 μm thick GaN film grown by MBE.

Homoepitaxially grown *pn*-junctions were fabricated by depositing an MBE grown p-GaN layer on these ELO-HVPE n-GaN templates. Prior to loading into the MBE, these templates were immersed in 50% HCl for 5 minutes followed by a DI-water rinse. Besides standard outgassing, no other *in- situ* cleaning of the substrates was done.

The growth of the active layers on the HVPE-grown GaN/sapphire proceeded directly without any plasma pretreatment. A top view of a fabricated device is shown in Figure 24. The p-mesa was formed by RIE using 20sccm of Cl_2 at a total pressure of 13 mTorr as a reactive gas. The total power in the discharge was 320W and the DC bias of the cathode was 750 volts. A 5μm Ni/Au bimetal film was used as an etch mask for mesa definition. Mesa sizes of 5μm X 20μm and 12μm x 160μm were defined. Subsequently, the Ni/Au etch mask was removed and narrow strips of Ni/Au (20nm/ 500nm) were deposited as *p*-ohmic contacts. Pressure contacts using a tungsten probe were used as *n*-type contacts.

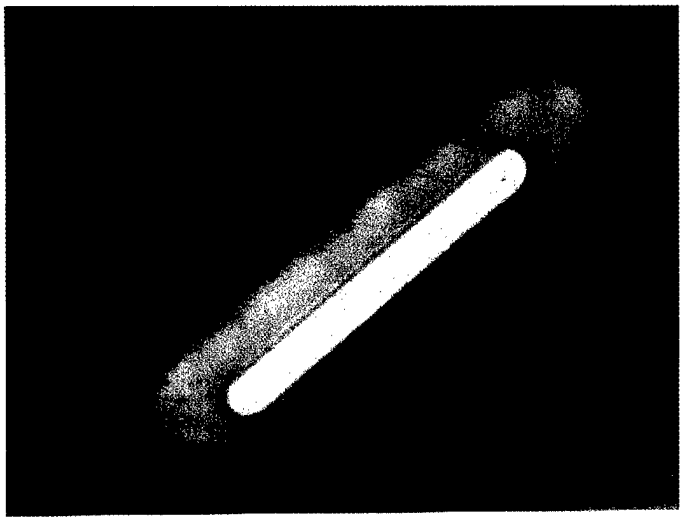

Figure 24. 12μm x160 μm ELO pn junction diode

Figure 25 shows the dark I-V characteristics for the ELO n^+ -GaN/ p- GaN diode. It is observed that this device is similar to a smaller device fabricated by the Santa Barbara group [7]. The leakage current in this device is about 2 orders of magnitude better than the homoepitaxial devices grown on bulk HVPE films whose IV characteristics are shown in Figure 21. Since the density of dislocations in the ELO-GaN film is $< 10^7$ cm^{-2}, we attribute this improvement to the reduction of threading dislocations in this device. The large forward series resistance in our device is attributed to contact resistivity in both the *n*- and *p*-type contacts.

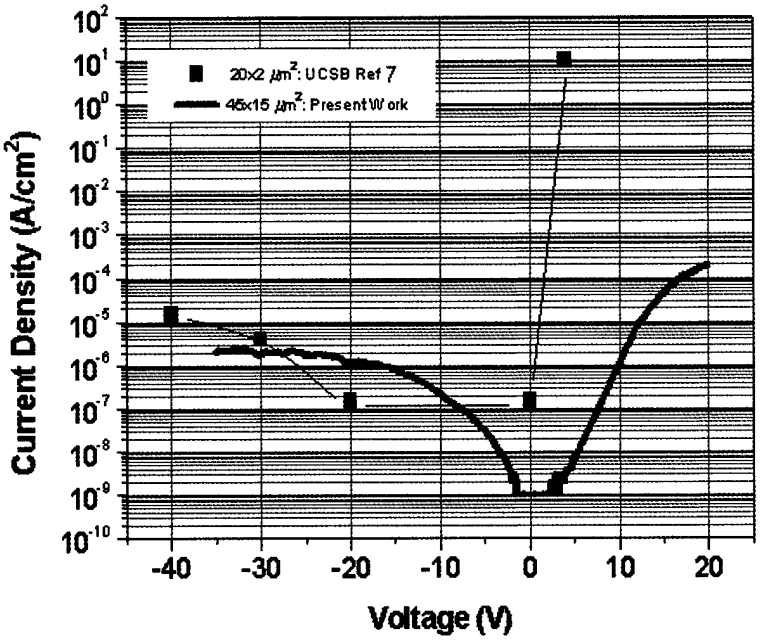

Figure 25. IV Characteristics of pn junction deposited on ELO-HVPE GaN template

2.6. Passivation of dislocations by annealing in H_2 atmosphere

Another method for reducing the leakage currents in these devices is to passivate the dislocations using H_2. Figure 26 shows the IV characteristics measured in the reversed direction for a heteroepitaxially grown, 300 μm diameter, GaN p-n junction diode before and after rapid thermal annealing (RTA) in a forming gas ambient (90% N_2:10% H_2) at 650 °C for 45 seconds. This annealing was done in an AGA Heatpulse 410 rapid thermal annealing furnace. A dramatic reduction in the reverse leak current of over 3 orders of magnitude is observed at low biases and at least 1 order of magnitude reductions is seen at higher biases. This reduction is attributed to the passivation of dangling bonds in the threading dislocations by hydrogen. It has also been observed that the effects of this passivation can be reversed by subsequently annealing the film in a N_2 ambient.

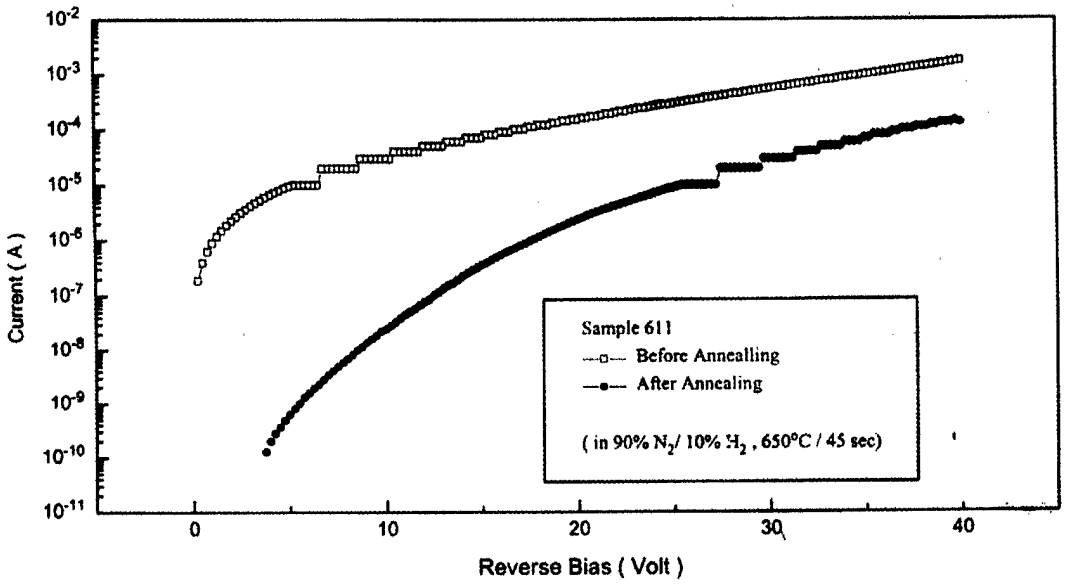

Figure 26. Reverse bias IV characteristics of GaN *pn*-junction before and after annealing in forming gas.

2.7 Optical characterization of *p-i-n* GaN detectors

The spectral response of heteroepitaxially grown on sapphire GaN *p-i-n* junctions have been studied and their responsivity, measured at the absorption edge, is presented as a function of applied bias in Figure 27. Theoretically, a p-n junction photodetector cannot have gain since a single photon absorbed in the depletion region can generate only a single e-h pair and therefore these devices may not have quantum efficiency greater than unity (.27 A/W for GaN based devices).

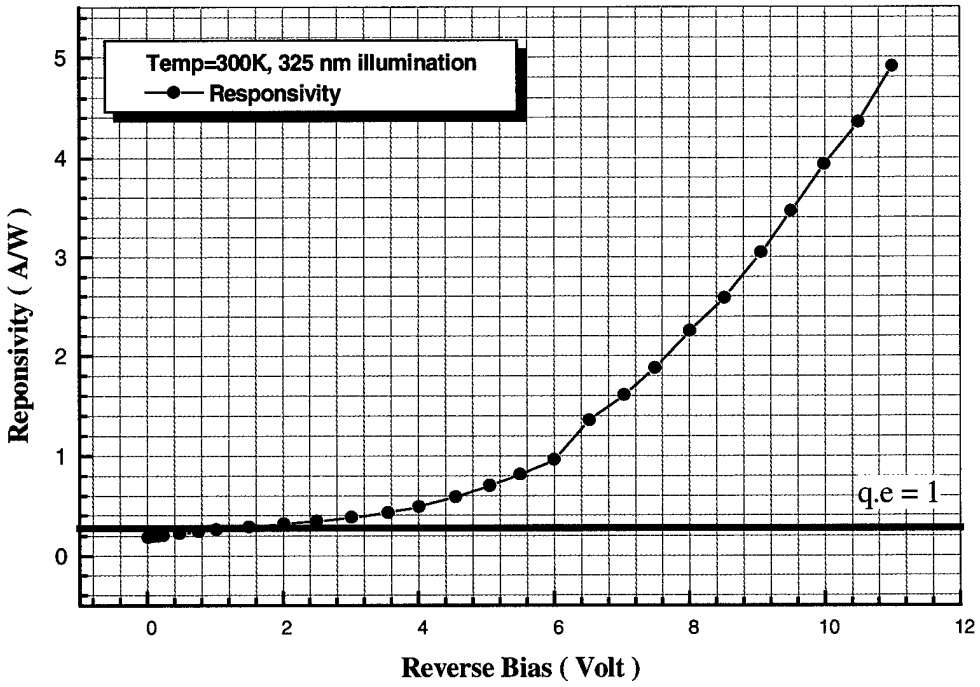

Figure 27. Responsivity of a heteroepitaxially grown p-i-n GaN junction as a function of bias.

This gain might be explained by the presence of defects in these materials and the depletion regions that surround them as shown schematically in Figure 28. The dislocations in these materials are charged and are known to deplete the material surrounding them. This material is then resistive and thus upon illumination the minority carriers can be trapped giving rise to a photoconductive gain. An equivalent circuit model for a semiconductor with threading dislocations would then be a resistor in parallel with the *p-n* junction diode as shown in Figure 28.

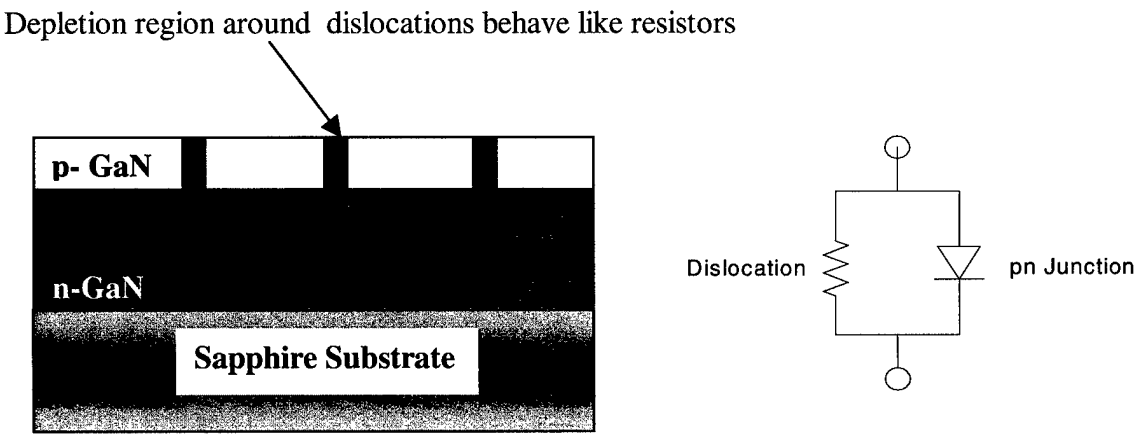

Figure 28. Schematic of a dislocation in a GaN *pn* junction and the equivalent circuit model

3. Conclusions

A number of materials studies of GaN and AlGaN alloys were undertaken towards the optimization of this class of materials for the fabrication of visible-blind and solar-blind UV detectors. Particular emphasis was place in the developing thick GaN templates by the halide vapor phase epitaxy method (HVPE) and epitaxial lateral overgrowth method (ELO-HVPE). These templates have densities of dislocations 10^7 cm^{-2} and thus they are ideal substrates for the fabrication of detectors with low dark noise. AlGaN alloys were grown and doped degenerately *n*-type with Si upto Al concentration of 50%. To control the stress in these AlGaN films, and thus eliminate cracks, we have grown such alloys using a number of AlN interlayers.

Fabrication methodologies have been developed for the growth of arrays of visible-blind and solar-blind detectors for front and back illumination. A number of detectors in the form of Schottky barrier and *p-n* and *p-i-n* configuration were fabricated and tested. Schottky barrier detectors in the form of n^+-GaN/ n^-GaN, grown directly on sapphire substrates, were found to have responsivity at 355 nm of 0.18 Amps/Watt, which corresponds to 70% quantum efficiency. The spectral response of these devices shows a sharp transition in the gap of the semiconductor (360 nm) of approximately five orders of magnitude. On the other hand, similar devices fabricated on n^+-HVPE GaN/ n^- MBE GaN were found to have only two and a half orders of magnitude visible light rejection and a long response tail extending to the middle of the band gap of the semiconductor. We attribute this long tail to absorption and collection of carriers in the thick HVPE-grown GaN template. P-n and p-i-n junctions grown homoepitaxially on HVPE GaN templates were found to have dark noise at low reverse bias voltage in the neighborhood of 10^{-12} to 10^{-11} Amps/cm^2, which was correlated by EBIC measurements with leakage though threading dislocations.

A method has been developed to passivate threading dislocations by annealing *p-n* junction devices in forming gas. We believe this annealing effect is due to passivation of dangling bonds in threading dislocations with hydrogen. We observed that in *p-i-n* junctions with relatively high dislocation density (grown heteroepitaxially on sapphire substrates) the responsivity increases with reverse bias to values as high as 5 Amps/Watt. We attribute this anomalous gain to a photoconductive contribution from the depleted regions around the threading dislocations. In other words, these regions behave as photoconductors connected in parallel to the junction region of the device.

4. Publications

1. T.D.Moustakas, "Growth of Wide-Band Gap Semiconductors by MBE" *in Critical Review of Gallium Nitride based Technologies, (SPIE, 2002)*

2. A.V. Sampath, E. Iliopoulos, A. Bhattacharyya, I. Friel, I. Sandeep, J. Cabalu and T.D. Moustakas, "Growth of III-Nitrides by MBE", *Electrochemical Society Proceedings, **Vol. 2002-3**, pp.46-57 (2002).*

3. A.V. Sampath, A. Bhattacharyya, I. Sandeep, H.M. Ng, E. Iliopoulos, T.D. Moustakas " MBE Growth of GaN using NH3 and Plasma Sources ", *Mat. Res. Soc. Symp. Proc.* Vol. **639**, G6.56.1 (2001)

4. T.D. Moustakas, E. Iliopoulos, A.V. Sampath, H.M. Ng, D. Doppalapudi, M. Misra, D. Korakakis, R. Singh, "Growth and Device Applications of III-Nitrides by MBE", J. of Crystal Growth, **227/228**, 13 (2001).

5. M. Misra, T. D. Moustakas. "Photoconductivity Recombination Kinetics in GaN Films." *Mat. Res. Soc. Symp.* Vol **622**, T5.4.1 (2000).

6. A. V. Sampath, M. Misra, K. Seth, Y. Fedyunin, H. M Ng, E. Illiopoulos, Z. Fiet and T. D. Moustakas "A Comparative Study of GaN diodes grown by MBE on sapphire and sapphire/HVPE-GaN substrate", *MRS Internet Journal of Nitride Semiconductor Research*, **5S1**, W11.1 (2000).

7. A.V.Sampath, E.Iliopoulos, K.Seth, M.Misra, H.M.Ng, P.Lamarre, Z.Feit, T.D. Moustakas "GaN photodiodes by MBE on HVPE and ELO-HVPE/Sapphire substrates in Photodetectors: Materials and Devices V– Proceedings of SPIE **3948**, 311 (2000).

8. M. Misra, A. V. Sampath and T. D. Moustakas "Investigation of vertical transport in n-GaN films grown by Molecular Beam Epitaxy using Schottky barrier diodes." *Appl. Phys. Lett.*, **76**, 1045 (2000)

9. M. Misra, A. V. Sampath and T. D. Moustakas "Vertical Transport Properties of GaN Schottky diodes Grown by molecular beam epitaxy", MRS Internet Journal Nitride Semiconductor Research, Res **5S1**, W11.2 (2000).

10. M.Misra, A.V.Sampath, E.Iliopoulos, T.D. Moustakas "GaN Schottky diode ultraviolet detectors grown by MBE" in Photodetectors: Materials and Devices V-Proceedings of SPIE **3948**, 342 (2000).

11. P. Ryan, Y.C. Chao, J. Downes, C. McGuiness, K.E. Smith, A.V. Sampath, T.D. Moustakas "Surface Electronic Structure of p-type GaN (0001)", *Surface. Science* **467**, L827 (2000).

12. M. Misra, D. Doppalapudi, A.V. Sampath, T.D. Moustakas, P.H. McDonald "Generation-Recombination noise in GaN Photoconducting detectors", *MRS Internet Journal of Nitride Semiconductor Research,* **4S1**, G7.8 (1999).

REFERENCES

1. K. Seth. M.S. Thesis (Boston University, 2000)

2. D. Doppalapudi, *et al.* in III-V Nitride Materials and Processes, ECS Proc Vol **98-18**, 87 (1999).

3. D. Korakakis, H. M. Ng, M. Misra, W. Grieshaber, T. D. Moustakas. MRS Internet Journal Nitride Semiconductor Researc, Vol **1**, No. 1-46, U81-U87 (1996).

4. A. Y. Polyakov, N. B. Smirnov, A. V. Govorkov, M. G. Milvidski, J. M. Redwing, M. G. Milvidski, J. M. Redwing, M. Shin, M. Skowronski, D. W. Greve, And R. G. Wilson. Solid State Electronics, **42**, 627 (1998).

5. H. Amano *et al.* Japanese Journal of Applied Physics, **37**, L1540 (1998).

6. S. Kamiyama *et al.* Japanese Journal of Applied Physics, **37**, L316 (1998).

7. M. Misra, A. V. Sampath, and T. D. Moustakas. APL 76, 1045 (2000).

8. C. Qui, C. Hoggatt, W. Melton, M. W. Leksono, and J. I. Pankove. APL, 66, 2712 (1995).

9. M. Misra, D. Korakakis, H. M. Ng, and T. D. Moustakas. APL, 74, 2203 (1999).

10. R. P. Vaudo and V.M. Phanse. Electrochemical Society Proceedings, Vol 98-18, Edited by T. D. Moustakas, S. E. Mohney, and S. J. Pearton (The Electrochemical Society, 1999).

11. P. Kozodoy, J. P. Ibbetson, H. Marchant, P. T. Fini, S. Keller, J. S. Speck, S. P. DenBaars, and U. K. Mishra. APL, 73, 975 (1998).